Phototactic Miniature Soft Robots with Terrain Adaptability

Tonghui Zhao, Wei Fang, Yangyang Fan, Zhiming Hu, Han Wu, Xi-Qiao Feng,* and Jiu-an Lv*

Miniature locomotive robots that can adaptively change shapes to accommodate to various terrains have technologically significant applications ranging from noninvasive operations, environmental monitoring, to biomedical devices. However, existing miniature robots face two practical bottlenecks: limited mobility and low robustness, which severely restrict their applicability. In this work, terrain-adaptive miniature soft robots that can be powered, guided, and maneuvered on challenging terrains by a versatile phototactic strategy are created. These robots, constructed by a rationally designed liquid crystal elastomer with powerful photomechanical actuation, enable self-actuation to generate autonomous and self-sustained rolling locomotion under constant near-infrared light stimuli without any on-off switching. They outperform previous light-driven miniature robots and exhibit exceptional terrain adaptability to traverse a diversity of simple and complex terrains, and even hybrid terrains with varying topology, mechanics, and rheology. The terrain-adaptive robots can directionally leap over hurdlers, and even exert high jumping to overcome high wall obstacle. It is envisioned that this proposed technique would enable the design of miniature mobile robots that can accommodate varying terrains and fulfill multiple tasks in unpredictable environments.

T. H. Zhao, Y. Y. Fan, Z. M. Hu, H. Wu, J.-a. Lv
Key Laboratory of 3D Micro/Nano Fabrication and Characterization of Zhejiang Province
School of Engineering
Westlake University
Hangzhou 310024, China
E-mail: lvjiuan@westlake.edu.cn
T. H. Zhao, Y. Y. Fan, Z. M. Hu, H. Wu, J.-a. Lv
Institute of Advanced Technology
Westlake Institute for Advanced Study
Hangzhou 310024, China
W. Fang, X.-Q. Feng
Institute of Biomechanics and Medical Engineering
AML
Department of Engineering Mechanics
Tsinghua University
Beijing 100084, China
E-mail: fengxq@tsinghua.edu.cn
W. Fang, X.-Q. Feng
State Key Laboratory of Tribology
Tsinghua University
Beijing 100084, China

1. Introduction

Untethered mobile robots miniaturized to the length scale of millimeters and below would have substantial scientific and technological impacts in numerous applications,[1,2] such as manipulating devices enabling operations performed in narrow and complex regions inaccessible for human eyes or hands, microfactories allowing the construction of 3D heterogeneous microparts,[3,4] and dynamic monitoring and surveillance through deploying robots to form mobile sensor networks.[5] However, poor mobility on real terrains, and low robustness to mechanical damage and environmental impact[6,7] have seriously hindered the development of existing miniature mobile robots. Generally, miniature mobile robots can be divided into two main types: rigid robots and soft robots, according to the elastic moduli of their constituent materials. The development of miniature rigid robots has been led by microelectromechanical systems (MEMS) technology,[8–10] which employs stiff materials (with an elastic modulus around 10^3–10^6 MPa)[11] such as polysilicon, metal, or hard plastics to construct the bodies, legs, links or hinges of robots, and their locomotion is driven by thermal, vibration, electrostatic, or piezoelectric actuation.[6,9,12] However, these previously reported robots are only applicable to locomotion in specific mild environments artificially constructed in experimental labs, and unable to negotiate obstacles and changes in the texture and materials of unstructured environments due to limited mobility resulted from low degrees of freedom.[3,4] Additionally, MEMS-based robots are prone to irreversible damage, due to their delicate structures and lower tolerance to deformation due to the fragility of these rigid materials.

In the recent years, miniature soft robots (MSRs) (with elastic modulus in the order of 10^{-2}–10^3 MPa)[13] made of hydrogels, shape-memory polymers, and elastomers have been increasingly expected to achieve higher mobility because they possess continuous compliant bodies capable of achieving infinite degrees of freedom (DOF).[14,15] These robots can be powered and controlled by various external stimuli, including temperature, electric or magnetic fields, light, acoustic waves, and chemical stimuli.[16] Light is an attractive contactless driving source with the salient feature of spatial, temporal, magnitude, directional tunability. Jiang et al. created near-infrared

**ADVANCED
SCIENCE NEWS**
www.advancedsciencenews.com

**ADVANCED
MATERIALS
TECHNOLOGIES**
www.advmattechnol.de

(NIR)-driven bilayer soft robots that exhibit swimming behaviors.[17] Palagi and colleagues devised microrobots that show biomimetic swimming manipulated by structured light.[18] Zeng et al. designed light-fueled walkers that allow directional walking, rotation, and jumping.[19] Rogoz et al. developed light-driven soft robots that mimic caterpillar locomotion.[20] Inspired by motion behaviors of soft worms, Ahn et al. prepared light-fueled soft robots that show diverse modes of locomotion including crawling, squeezing, and jumping.[21] Locomotion performances of representative light-driven soft robots reported over the last few years have been summarized in Table S2 (Supporting Information). Despite these exiting progresses, existing light-driven MSRs largely only adapt to simple and flat terrains constructed in labs, since the manipulation of flexible soft robots to gain desirable locomotion behavior to negotiate varying environments is extremely challenging because of highly nonlinear mechanical properties of soft materials.[22,23]

In nature, small limbless organisms exhibit remarkable capabilities to manipulate their soft bodies to gain versatile mobility and adaptation in varying environments. For example, *Drosophila larva* can not only control its soft body to crawl forward and backward, but also achieve lateral rolling (**Figure 1**a), and even jumping locomotion, which allow them to efficiently traverse across various terrains and rapidly escape away from predators or noxious environmental stimuli.[24,25] To achieve these functions, larva need manipulate hundreds of muscles, each individually addressed and powered in a coordinated manner to dynamically deform and morph its soft body to produce desired locomotion.[26,27] However, integration and control of hundreds of discrete muscle-like actuators in a synthetic soft robot are a great challenge,[28] especially when its length scale must be miniaturized to millimeters or even smaller.[18,29–31]

Here, we present a conceptually novel phototactic strategy to remotely power, steer, and maneuver untethered millimeter-scale soft robots constructed of NIR-active liquid crystal elastomer. The robots with a virtually unlimited number of DOFs can be actuated and steered by NIR light to generate time-varying shapes, and thus they can undergo autonomous, directional rolling on diverse terrains, and flexibly switch locomotive modes (rolling, leaping, somersaulting, and high jumping) to adapt to negotiate various obstacles. Unlike previous light-driven miniature mobile robots, the design and phototactic guide strategy of the proposed all-terrain miniature soft robots (ATMSRs) can achieve multilocomotive functions with a superior robustness and terrain adaptability.

2. Results and Discussion

2.1. Principle of ATMSR System

As a kind of smart deformable polymers, photoactive liquid crystal elastomers (PLCEs) exhibit dynamic and reversible shape-morphing through phototriggered change in the liquid crystal (LC) director field, and allow remote powering, spatiotemporal control, and dynamic reconfigurability, and thus enable unlimited number of DOFs.[16,32,33] Hence, PLCEs are suitable to construct untethered miniature mobile robots.[16] Distinguished from previous LCE-based robots that define the

locomotive mode once through predetermine programming pattern of the director orientation field, we employ an alternative straightforward and versatile strategy which uses directional light to gain dynamic time-varying shape-morphing and to create diverse locomotive modes in a single soft robot with uniform director orientation. The shape-morphing and locomotive modes can be prescribed dynamically, and do not require preprogramming of the LC director field. For the ATMSRs, LC mesogens serve as molecular-sized actuators and self-assemble into the continuously deformable body of an ATMSR, and these tiny actuators can be independently fueled and manipulated by actinic light, providing an efficient approach to synchronously achieve remote power, spatiotemporal actuation, and programmable control. Thus, ATMSRs are capable of continuous and dynamic reprogrammed locomotive modes in real time through controllable directional illumination, realizing infinite flexibility, and exceptional adaptation.

2.2. Phototactic Control of ATMSRs

The photoactive, rectangular-sheet-shaped, ATMSRs (Figure 1b) are fabricated using the procedures described in the Experimental Section. To gain powerful actuation of ATMSRs, a NIR-responsive main-chain liquid crystal elastomer (NIR-MLCE) has been designed with two considerations: the main-chain structure of NIR-MLCE enhances mechanical output and NIR response offers environment-friendly, biocompatible, and contactless response (Figure 1c). In these ATMSRs, the covalently bonded NIR groups absorb 808 nm light (Figure 1d), triggering the dynamical morphing of ATMSRs, which is employed to produce desired locomotion. As shown in Figure 1f,g, directional rolling locomotion has been generated and readily control by modulation of incident NIR. When a rectangular-shaped NIR spot with the long axis parallel to that of the ATMSR is utilized to illuminate the robot from one lateral side (Route 1 in Figure 1e), it starts autonomous and self-sustained rolling (Route 1 in Figure 1f,g1; and Part 1 of Movie S1, Supporting Information), while, when illuminated from the other lateral side, the robot can also start the rolling but reverse the moving direction (Route 2 in Figure 1f,g2; and Part 2 of Movie S1, Supporting Information). To gain directional turning in the rolling locomotion, a tilted NIR spot is used to illuminate one lateral side of an ATMSR, and turning direction is fully controlled by two factors: the tilted NIR direction, and the illuminated side of the ATMSR. As shown in Figure 1e, a clockwise tilted NIR spot illuminates the left lateral side of the robot, triggering turning locomotion toward the northwest (Route 3 in Figure 1f,g3; and Part 3 of Movie S1, Supporting Information) while an anticlockwise tilted NIR spot illuminates the same lateral side, leading to turning locomotion toward the southwest (Route 4 in Figure 1f,g4; and Part 4 of Movie S1, Supporting Information). When the right lateral side of the ATMSR is illuminated by either an anticlockwise or clockwise titled NIR spot, the direction of turning can be totally controlled to the northeast (Route 5 in Figure 1f,g5; and Part 5 of Movie S1, Supporting Information) or southeast (Route 6 in Figure 1f,g6; and Part 6 of Movie S1, Supporting Information). In this report, the rolling locomotion is triggered via illuminating from one lateral side of
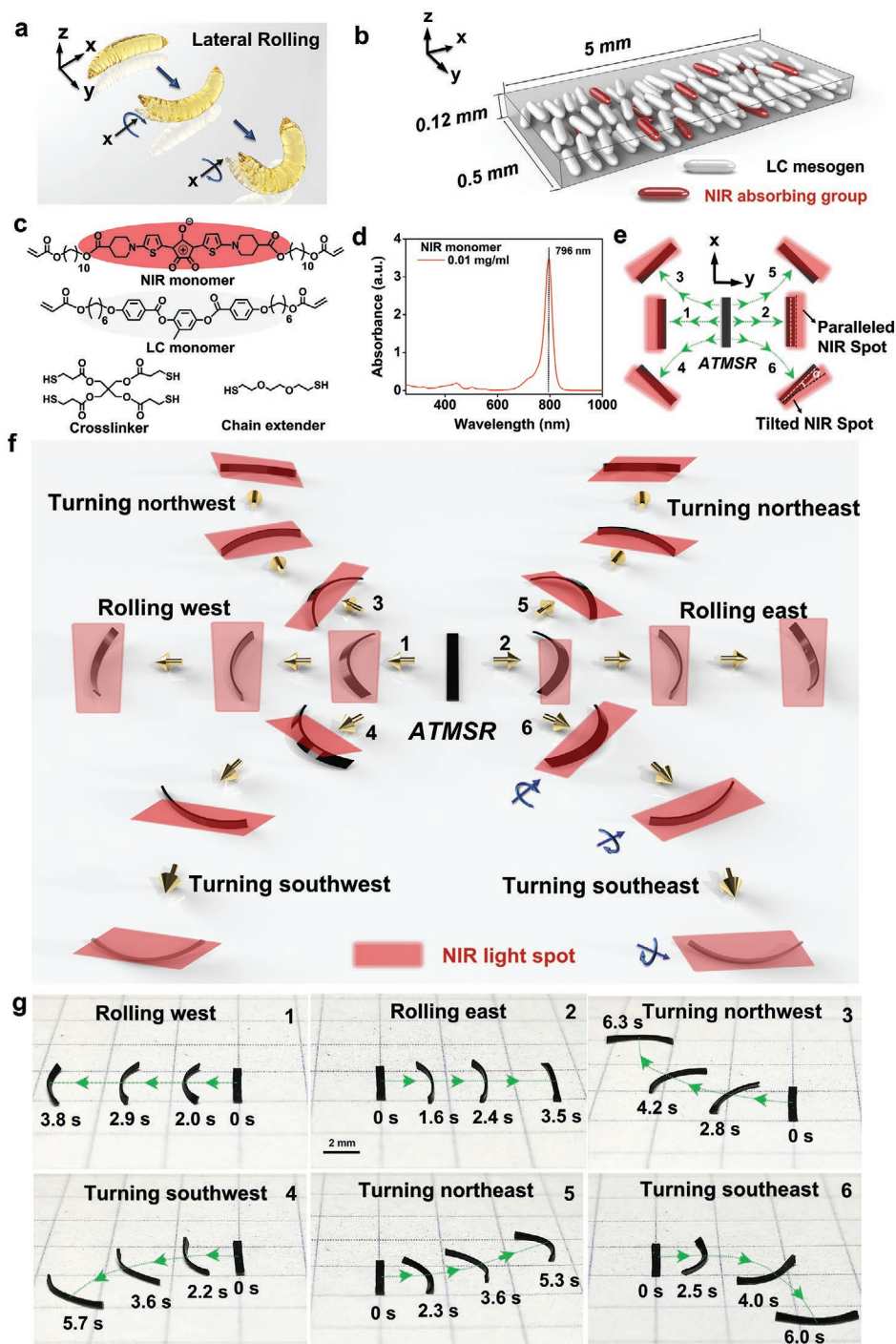
Figure 1. Phototactic manipulation of ATMSR. a) Schematics showing the lateral rolling locomotion of *Drosophila larva*. b) Dimensions and LC orientation profile of the rectangular-sheet-shaped photoactive ATMSR. LCs are orientated along the *y* direction. White and red rods represent LCs and NIR absorbing groups, respectively. c) Molecular structures used for fabrication of ATMSR. d) Absorption spectrum of the synthesized NIR monomer. e) Schematics showing the phototactic strategy to gain directional rolling (top view). The white dash line and black dashed line indicates the long axis of the ATMSR and the rectangular-shaped NIR spot, respectively. α indicates the angle between the long axis of the ATMSR and the spot. f) Schematics showing light-driven direction rolling of an ATMSR. The numbers from **1** to **6** represent the moving routes of straight rolling toward west (**1**) and east (**2**), turning northwest (**3**), southwest (**4**), northeast (**5**) and southeast (**6**), respectively. The red patterns denote the shape and location of the moving NIR light spot that was fully covering and following the rolling ATMSR to power and drive the rolling locomotion. The gold arrows indicate moving directions of the rolling ATMSR and the moving NIR light spot. g) lateral photographs experimentally showing directional rolling of ATMSR. A rectangular-shaped NIR spot with controlled orientation is used to power and steer ATMSR. When the NIR spot, whose long axis is parallel to that of ATMSR, illuminates from one lateral side of ATMSR e-1), it starts rolling straight following the forward moving spot (Route 1 in f,g; and Part 1 of

the ATMSR. Once triggered, the ATMSR can conduct autonomous and self-sustained rolling locomotion under constant and continuous NIR radiation, whereas existing light-driven soft robots largely rely on on-and-off switch of light stimuli to gain locomotion, which severely lacks autonomy.

2.3. Terrain-Adaptive Mobility

Mobile robots venturing out of the laboratory and interacting with the natural environment should possess terrestrial adaptability over varied ground with diverse topological, and mechanical features.[34–36] ATMSRs exhibit remarkable capabilities not only to rapidly roll across various flat terrains (glass, steel, wood, draft paper, rubber, and fabric surface) regardless of rigid or soft properties, low or high friction (Figure S1 and Movie S2, Supporting Information), but also effectively move across complex terrains such as gravel road, metal mesh, air bubble wrap sheet, polyethylene (PE) foam surface, bristle tips, to soil and desert sand (**Figure 2**a,b; and Figure S2a–e and Movie S3, Supporting Information), which can often be uneven, sloped, low contact area, and even flowable. The mobility on such complex terrains is much higher than that on flat terrains.[34,36,37] Moreover, by functionalizing the surface of ATMSRs with a thin layer of superhydrophobic silica, ATMSRs can be engineered to enhance their surface hydrophobicity which enable them to effectively traverse across hybrid (fluid-solid) terrains such as dewy glass surface, wet, and rough rock, even mud pool (Figure 2c; and Figure S2f (Supporting Information); Figure 2d; and Movie S4, Supporting Information). Traversing hybrid terrains is challenging for miniature mobile robots,[38,39] because small-sized robots are prone to firmly adhere on the wet ground and lost their mobility due to strong capillary forces arising from capillary bridges between the robot and the ground. Furthermore, the locomotion on all complex terrains would be subjected to static and dynamic instability and translational and rotational perturbations, and thus the robots may suffer from loss of foothold and an inability to generate appropriate ground reaction forces,[40,41] which significantly interfere with the mobility of existing miniature mobile robots.

In addition, sloping terrains that insects often encounter in nature, however, are challenging for existing light-driven miniature soft robots. In previous reports,[42] special designs of inclined planes, for example, by introducing a ratcheted surface, have been required to provide the friction bias for uphill motion of the light-driven soft robots. It is difficult to rapidly climb up a flat and slippery glass incline with low friction,[43] the fastest records showed an uphill motion with a velocity of ≈0.2 mm s^{-1} on 15° incline,[44] while the outstanding ability to climb on an inclined surface with a tilting degree of up to 30° with a

speed of ≈0.002 mm s^{-1} was reported.[45] However, the ATMSRs exhibit a superior ability to roll up a 20° incline of flat slippery glass with a velocity up to ≈1.43 mm s^{-1} (Figure 2e; and Part 1 of Movie S5, Supporting Information). More impressively, the ATMSRs can rapidly run upstairs at a high moving speed of ≈5.1 mm s^{-1} (Figure 2f; and Part 2 of Movie S5, Supporting Information), and even ascend an ≈13° sand incline with a velocity of ≈0.71 mm s^{-1} (Figure 2g; and Part 3 of Movie S5, Supporting Information). Sand incline with frequently compliant ground that can yield and flow, producing complex and dynamic interactions, and resulting in slip and penetration of the moving robot,[36] which often leads to the failure in uphill for existing mobile robots.

2.4. Mechanism of Rolling Locomotion

The above locomotive behaviors of ATMSRs all arise from their high capacity of anisotropic deformation in response to NIR light (**Figure 3**a). As is well known, liquid crystal mesogens in LCEs possess orientational order whose local direction and strength are characterized by the nematic director n and the order parameter S.[18] The S-value of LCEs is inversely proportional to temperature (Figure S3a, Supporting Information). The NIR groups absorbs NIR light that causes the temperature rise of NIR-MLCE (Figure S3b, Supporting Information). For the uniaxially oriented LCEs, the temperature increase leads to the decrease in S, triggering anisotropic deformation consisting of contraction along the direction parallel to n, while expansion along the direction perpendicular to n (Figure 3a; and Figure S3c, Supporting Information). To figure out the rolling mechanism of ATMSR(s), the slow-motion video recorded by high-speed camera enables us to clearly observe shape changes during rolling (Figure 3b,c; and Movie S6, Supporting Information). We use a light-heat-mechanical coupling model to numerically visualize the spatial distribution and intensity of NIR-induced temperature changes on the ATMSR (Figure 3d; and Figure S3d–f, Supporting Information). Thermal imaging of a rolling ATMSR clearly shows the temperature distributions and changes in rolling locomotion (Figure 3e; and Movie S7, Supporting Information).

The temperature gradients bring a spatially varying strain field, which determines the dynamic morphing of the ATMSR. The continuous cyclic rolling motion is caused by photoinduced deformation overcoming gravitational potential energy and further converting it into kinetic energy. As indicated by the color gradient (Figure 3d1), an increasing temperature gradient along the γ direction on the robot's upper surface (S1) is induced when the incident NIR light is illuminating an ATMSR from one lateral side, corresponding to a negative temperature gradient

Movie S1, Supporting Information). Illuminating from the other lateral side e-2) of the ATMSR leads to reverse the rolling direction (Route 2 in f,g; and Part 2 of Movie S1, Supporting Information). To gain directional turning of a rolling ATMSR, a tilted NIR spot is used to illuminate from one lateral side of the ATMSR, and turning direction is fully controlled by two factors: one is the tilted direction of the NIR spot, and the other is which later side of the ATMSR is initially chosen to be illuminated 1e). A clockwise tilted NIR spot illuminates from the left lateral side of the robot e-3), triggering turning locomotion toward the northwest (Route 3 in f,g; and Part 3 of Movie S1, Supporting Information) while an anticlockwise tilted NIR spot illuminates from the same lateral side e-4), leading to turning locomotion toward the southwest (route 4 in f,g; and Part 4 of Movie S1, Supporting Information). When the right lateral side of the robot is illuminated by either an anticlockwise e-5) or clockwise tilted NIR spot e-6), the turning direction can be totally controlled to northeast (route 5 in f,g; and Part 5 of Movie S1, Supporting Information) or southeast (route 6 in f,g; and Part 6 of Movie S1, Supporting Information). The green dashed lines represent the moving trajectory. The size of the ATMSR is 5 × 0.5 × 0.12 mm^3.
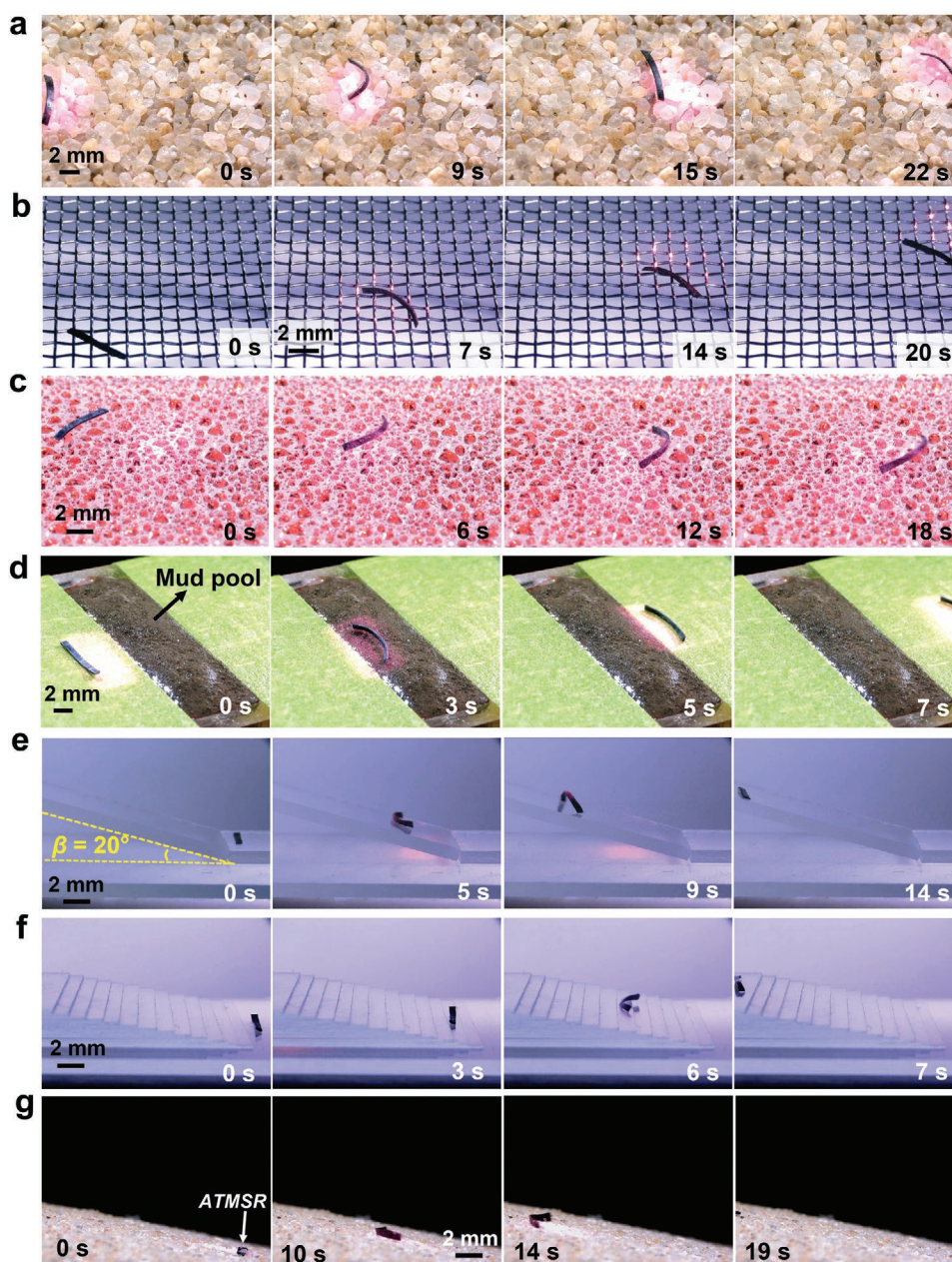
Figure 2. Adaptive mobility of ATMSR on various challenging terrains. a,b) Optical photographs demonstrating the versatile mobility of an ATMSR on rocky terrain a) and meshed terrain b), respectively (Movie S3, Supporting Information). The metal square wire mesh with a hole size of $1.2 \times 1.2 \ mm^2$ and a wire diameter of ≈ 0.2 mm. c) Lateral photographs showing light-driven locomotion of an ATMSR on a hybrid liquids–solid terrain formed by spraying water droplets on glass substrate (Part 1 of Movie S4, Supporting Information). The sprayed water forming many sessile drops makes the glass substrate strong adhesive for small objects. A red dye was dissolved in the water to improve visibility of the sessile drops. d) Lateral photographs showing photocontrol of an ATMSR traversing across a complex hybrid terrain of mud pool (Part 3 of Movie S4, Supporting Information). e) Lateral photographs showing light-driven uphill locomotion of an ATMSR on a glass incline tilted up to $\beta = 20°$ (Part 1 of Movie S5, Supporting Information). f) Lateral photographs showing light-driven uphill running of an ATMSR on a stair incline (Part 2 of Movie S5, Supporting Information). The height of each stair is ≈ 0.21 mm. g) Lateral photographs showing light-driven uphill locomotion of an ATMSR on a sand incline of $\approx 13°$ (Part 3 of Movie S5, Supporting Information). The size of the ATMSR is $5 \times 0.5 \times 0.12 \ mm^3$. The intensity of the 808 nm light source is 0.8–3 W cm^{-2}.

along the z direction (Figure 3d2). The temperature gradients along the two directions produce the variation in the orientational order, which in turn results in both lateral (Figure 3f) and forward bending (Figure 3g) simultaneously. As shown in the image **2** of Figure 3b,c, the overall light-induced deformation

of the ATMSR features nonplane bending (Figure S3g,h, Supporting Information). Such asymmetric bending deformation makes the ATMSR lose its balance and topple down (Image **2–3** in Figure 3b,c). In this toppling down, the lateral side CD is moving away from the NIR source, while the lateral side AB
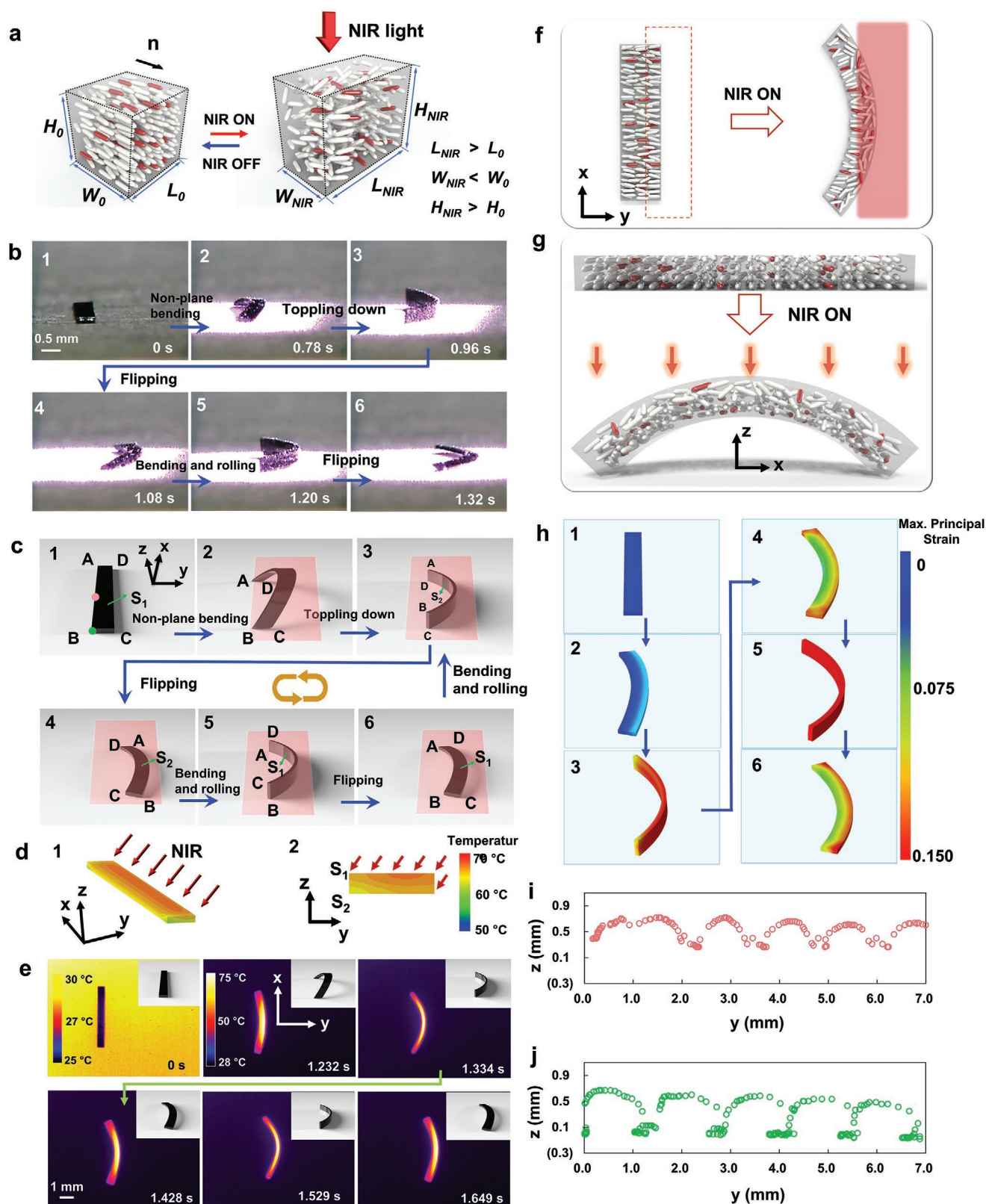
Figure 3. Mechanism of rolling locomotion. a) Schematics showing NIR-light induced anisotropic deformation of an uniaxially oriented LCE. For uniaxially oriented LCEs, the increase of NIR-induced temperature leads to the decrease in the orientational order, triggering anisotropic deformation: contraction along the direction parallel to the nematic director n, while expansion along the direction perpendicular to n. b,c) Experimental (b, lateral view, Movie S6, Supporting Information) and schematics photographs (c, lateral view) showing sequential snapshots of the rolling locomotion upon

of the ATMSR is gradually facing the light source, leading to a fading of the temperature gradients along the y direction. As a result, the lateral bending gradually vanishes, while the forward bending is enhanced, and then the ATMSR rotates 90° around the x axis (Figure S4a2,a3, Supporting Information) and rapidly forms an arched state (Image 3 of Figure 3b,c). Thereafter, the lateral side AB of the robot becomes closer to the light source than the lateral side CD, yielding a greater photothermal elongation along the side AB. This asymmetrical deformation, together with the inertia of the rolling, drive the ATMSR to flip and rotate another 90°. At this state, its upper surface (S_1) turns back to the light source while its lower surface (S_2) faces the light source (Figure S4b,c, Supporting Information). When the flipping finishes, the ATMSR shows a lying lateral bending shape (Figure 3b-4,c-4). This test remarkably shows that, under the constant light irradiation, the lateral bending and the subsequent front bending make the rapid morphological transition from the lying state to the arched state, driving the ATMSR to rotate the third 90° (Figure S4d-4–d-m, and S4e, Supporting Information). Then the ATMSR flips again, conducts the fourth 90° rotation as described like above, and completes a cycle of 360° lateral rolling.

The ATMSR can repeat the cycle loop of **6-3-4-5-6** (Figure 3c) and thus keep autonomous rolling upon NIR irradiation. Our finite element simulations precisely visualize the distribution and intensity of the spatial distribution of the light-induced strains and the resulted time-varying shapes that drive the directional rolling of the ATMSR (Figure 3h). It is worth emphasizing that the lateral rolling of the ATMSRs depends mainly on the light-triggered dynamic morphing and the gravity-induced motion, whereas friction is only required to induce the forward locomotion when rolling.

2.5. Rolling Kinematics

To figure out the mechanisms behind the remarkable all-terrain adaptability described above, we perform a kinematic analysis of the rolling locomotion of the ATMSR. Two marked points, as shown in Figure 3c1, are tracked to determine their moving trajectory, amplitude, and speed. The trajectory profiles (Figure 3i,j) suggest that the two tracked points behaves mechanically as though they are riding on a Spring-Loaded Inverted Pendulum (SLIP).[46] Such swift locomotive behavior is attributed to the periodic varying displacements in both the horizontal and the vertical directions over time (Figure 3b), the maximum displacements of the tracked green point along the x

and z-axes are about ≈2.8 and ≈0.6 mm within a 360° lateral rolling cycle, respectively. The moving displacement along the z-axis enables the ATMSRs to scale obstacles during the rolling locomotion. Moreover, the ATMSR uses a regularly symmetrical alternating gait in a highly maneuverable and robust manner (Figure S5a–c, Supporting Information). In this locomotion gait, the two ends and lateral sides of the robot alternatively contact the ground (Figure S5b,c, Supporting Information), whereas the majority of its surface does not, which can effectively reduce frictional resistance to locomotion. Figure 3i,j also demonstrates the trajectory of "bouncing" gait with periodic deceleration and following acceleration in both the vertical and horizontal direction (Figure S5d,e, Supporting Information). Mounting evidence in biomechanics have suggested that agile locomotion in nature is organized by recourse to a controlled bouncing gait.[47] Both SLIP-like moving trajectory and bouncing gait are beneficial for ATMSRs to effectively traverse a wide diversity of terrains.

2.6. Light-Driven Actuation

Our photomechanical experiment demonstrates that ATMSRs possess powerful actuation stress up to ≈1.6 MPa (Figure S6a, Supporting Information), which is four times higher than the actuation stress in skeletal muscles (≈0.35 MPa).[48] Figure S6b,c (Supporting Information) demonstrates that an ATMSR can lift an ultraheavy load more than 24 456 times its own weight (Movie S8, Supporting Information). The highest record in previously reports shows a photoactive LCE lifting a load 5600 times heavier than its own weight.[49] Moreover, Figure S6d (Supporting Information) demonstrates that a square ATMSR undergoes 39% contraction along the director **n** and 34% expansion along its perpendicular direction when **S** decreased from 0.69 to 0.23 upon 808 nm NIR irradiation. After turning off the light source, the ATMSR quickly self-returns to the initial shape without any aid of light or other stimuli. Such reversible deformation on the intermittent irradiation with 808 nm light can be repeated over hundreds of cycles without obvious fatigue, because of strong chemical crosslinked network of the used ATMSR material.

2.7. Ultrarobustness

Robustness is crucial for the survival of mobile robots in performing practical tasks in different conditions.[7,50] The

NIR irradiation. First, out-plane bending was induced by the irradiation of NIR light from one lateral side of the ATMSR (b1–b2 and c1–c2), leading the ATMSR lost its balance and result in lateral rotation of 90° (b2–b3, c2–c3). Next, the ATMSR flips and rotates another 90° (b3–b4, c3–c4), and after the flipping, then it generates a weak out-of-plane bending (b4 and c4). And then, the lateral bending of the ATMSR vanishes, while the front bending is enhanced, the ATMSR conducts the third 90° rotation (b4–b5, c4–c5). Next, the bending ATMSR rotates the fourth 90° and flips again. Thus, the ATMSR completes one 360° lateral rolling. d) Simulation showing spatial temperature gradients in the ATMSR that is illuminated by incident NIR light from its lateral side. d1 and d2 show the temperature distribution in 3D model and the cross section of the ATMSR, respectively. e) Thermal imaging of a rolling ATMSR upon NIR irradiation (top view) (Movie S7, Supporting Information). The insets at the top right of the images schematically show the corresponding light-induced morphing of the rolling ATMSR (lateral view). f,g) Schematics showing the light-induced directional bending of the ATMSR toward the y direction (f, lateral bending, top view) and z direction (g, front bending, lateral view), respectively. White and red bars represent the liquid crystal mesogens and NIR absorbing groups, respectively. h) Simulation showing spatial strain gradients and resulted time-varying shapes of the ATMSR upon NIR irradiation. i,j) 2D trajectory of the marked red point and green point on the ATMSR during the lateral rolling, respectively. The time interval between each two adjacent data points is 8 ms. The location of the marked points is shown in c 1).
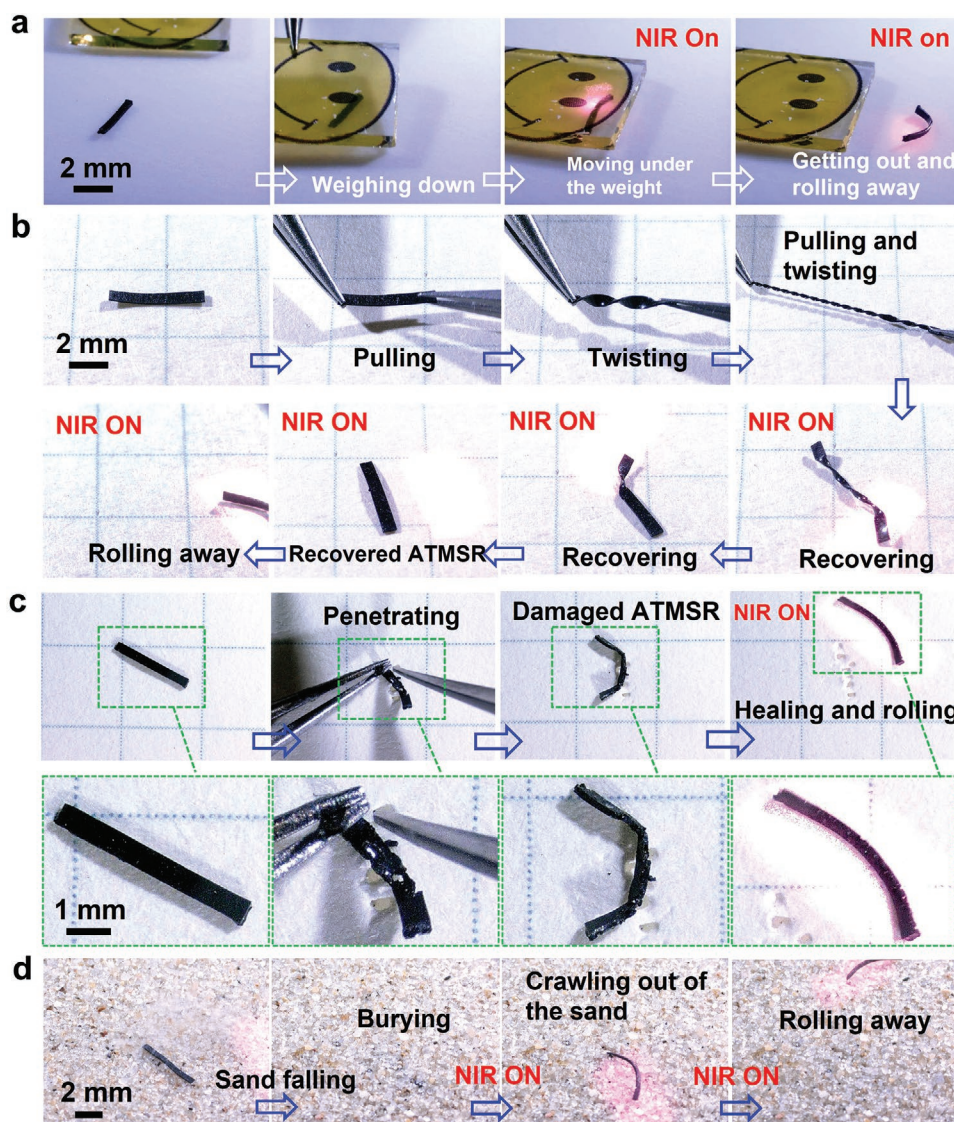
Figure 4. Ultrarobustness of ATMSRs. a) Photographs showing light-driven mobility of an ATMSR (0.26 mg) pressed under a heavy glass sheet (379 mg). The ATMSR can even move and turn when pressed under a heavy sheet, and it enable to crawl out the heavy sheet and roll away (Part 1 of Movie S9, Supporting Information). b) Photographs showing rapid self-repairing and mobility restoration of an ATMSR after severe distortion caused by rigorously mechanical pulling and twisting (Part 1 of Movie S10, Supporting Information). An ATMSR was manually pulled and twisted by two tweezers that grip the two ends of the ATMSR. The distorted ATMSR self-repaired to the flat state upon NIR irradiation and regain its rolling mobility. c) Photographs showing rapid self-repairing and mobility restoration of an ATMSR after violently penetration. An ATMSR was gripped by a tweezer and penetrated by a metal awl. Although the violent penetration caused obvious broken holes and severe deformation to the ATMSR, it can self-repair within several seconds and restore its mobility upon NIR irradiation (Part 2 of Movie S10, Supporting Information). d) Photographs showing the buried robot by falling sand getting out the covered sand and rolling away out of the camera's vision (Movie S12, Supporting Information). It is simulated that an ATMSR encountered sand and dust weather, buried and trapped by falling sand. The ATMSR can extricate itself from the trap and retain its mobility. The size of the ATMSR is $5 \times 0.5 \times 0.12$ mm^3. The intensity of the 808 nm light source is 0.8–3 W cm^{-2}.

proposed ATMSRs demonstrate exceptional robustness. As shown in **Figure 4**a, even though an ATMSR (≈0.26 mg) is pressed down by a dumped plate (379.2 mg) that is more than 1400 times heavier than the ATMSR, and it can still move and successfully escape out from the super-heavy plate (Part 1 of Movie S9, Supporting Information). It also enables 360° turning motion under a pile of glass sheets (≈638 mg), which is 2453 times heavier than its own weight (Figure S7a; and Part 2 of Movie S9, Supporting Information). More importantly,

ATMSRs show an unprecedented capability to self-repair and restore its mobility rapidly if severe mechanical damage or impact occurs. As shown in Figure 4b,c; and Figure S7b (Movie S10, Supporting Information), when damaged by either extensively pulling and twisting, violently penetrating, or vigorously mechanical rubbing, the ATMSRs can rapidly self-repair within a few seconds upon light irradiation and rapidly regained its mobility. In addition, we demonstrate that the ATMSRs can still sustain its superior mobility even if they were highly
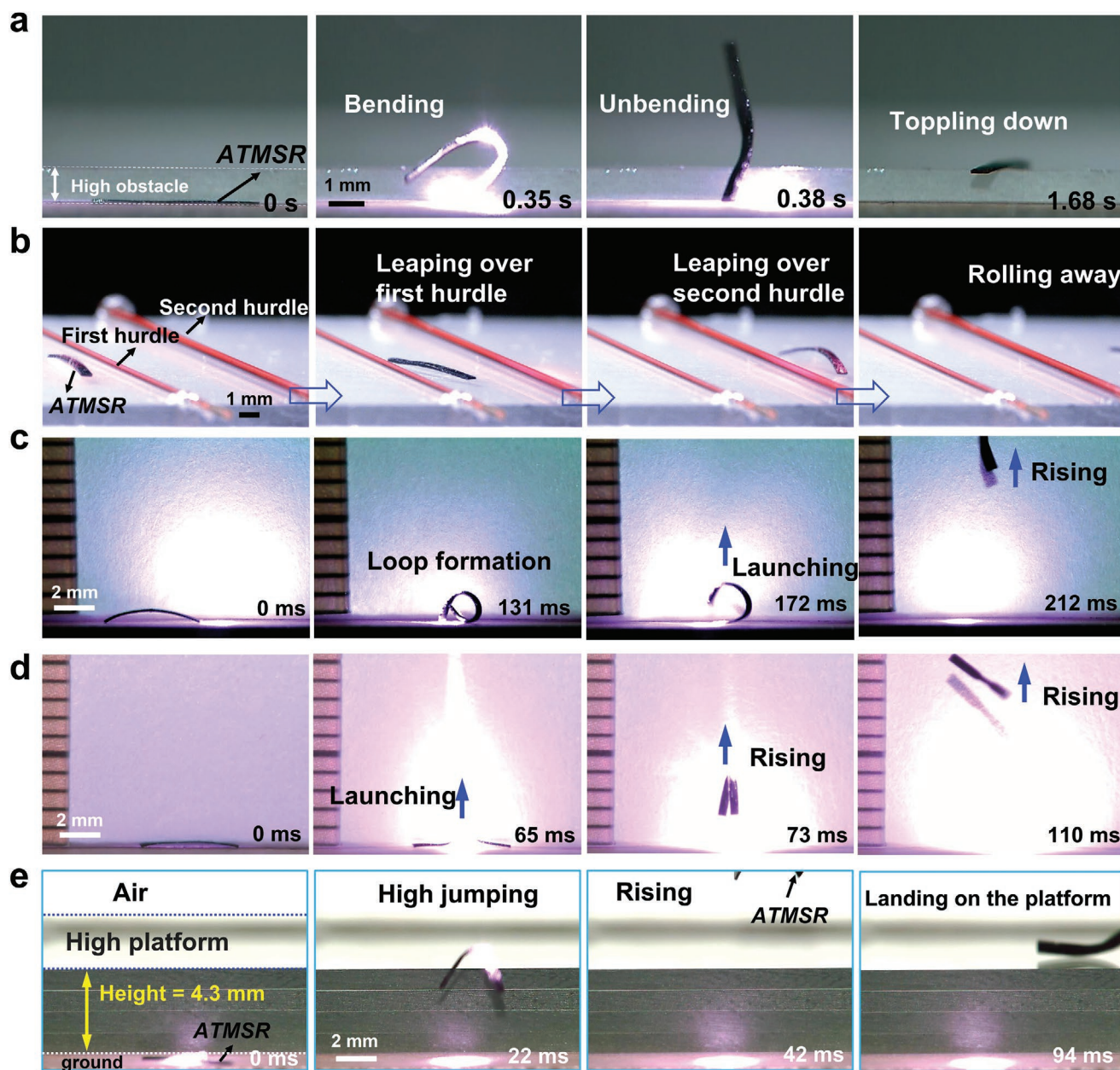
**ADVANCED
SCIENCE NEWS**

www.advancedsciencenews.com

**ADVANCED
MATERIALS
TECHNOLOGIES**

www.advmattechnol.de

Figure 5. Rapid movement of ATMSRs. a) Experimental photographs showing a light-driven rapid action like "pole vaulting" of an ATMSR (Part 1 of Movie S14, Supporting Information). When an ATMSR is illuminated by a moving NIR spot. The ATMSR exhibits a standing forward bend, and next unbend to stand upright and then topple down to get on the top of the high obstacle. b) Photographs showing phototactic steering of the ATMSR leaping over two rod hurdles (Movie S15, Supporting Information). The height of the two rod hurdles is 0.34 and 0.53 mm, respectively. c Snapshots showing light-driven latched high-jumping of an ATMSR (Part 1 of Movie S16, Supporting Information). A moving NIR spot is approaching one end of the ATMSR, the end of its body bends downward and curves into a C-shape, and the other end slides toward the curved end, forming a circular loop held together by a latch mechanism. As the light-induced deformation of the loop of the ATMSR is growing, sudden opening of "the latch" of the loop drives the ATMSR jumping up. d) Snapshots exhibiting buckling-induced high jumping driven by NIR light (Part 2 of Movie S16, Supporting Information). e) Snapshots showing photocontrol of an ATMSR jumping high enough to the top of a platform (4.3 mm) which ≈36 times higher than the height of the ATMSR (0.12 mm) (Part 3 of Movie S16, Supporting Information). In the third image of e), the ATMSR jumped too high, which lead it moving out of the camera's field of view. The size of the ATMSR is $5 \times 0.5 \times 0.12$ mm³.

stained and covered by contaminants such as soil (Figure S7c,d; and Movie S11, Supporting Information). Moreover, in the outdoor environment, dust or sand weather is unfavorable for the mobility of miniature robots. It is encouraging that, even in the extreme situation that ATMSRs are buried by a layer of sand or dust, they can break out of the atop sand upon light irradiation and restore its mobility (Figure 4d; and Movie S12, Supporting Information). All these ultrarobustness features make ATMSRs promising for adaption of working in harsh and unpredictable environments.[14]

2.8. Steering

In nature, small terrestrial organisms such as *Drosophila larvae* can flexibly adjust their moving direction to avoid obstacles or noxious environmental stimuli.[51,52] However, flexible control of locomotive directions remains a difficult task to achieve in synthetic light-driven soft robots (LSRs). As a result, most previous LSRs can only make forward and backward locomotion, and few have the ability of multidirectional locomotion.[20,53] As shown in Figure S8a (Supporting Information), an ATMSR can be guided to move along a curved path by alternating forward rolling and turning maneuvers, in an average speed of ≈1.2 mm s^{-1}. For illustration, we guided directional rolling of an ATMSR to transversely pass over a deep gap of width 1.25 mm (Figure S8b,c, Supporting Information). Moreover, the ATMSR can achieve rolling locomotion at a high velocity up to ≈6.5 mm s^{-1} (Movie S13, Supporting Information), breaking the fastest speed record of 3–5 mm s^{-1} of their nature prototype – *Drosophila Larvae*.[25] Under irradiation of the NIR light, the ATMSRs can keep a continuous and self-sustained rolling speed, without speed loss with time. Therefore, they can perform a moving task with a sufficiently long distance. Moreover, their rolling speed can be readily tuned from 0 to 6.5 mm s^{-1} by adjusting the intensity of light source from 0 to 1.52 W cm^{-2} (Figure S8d, Supporting Information). The turning degree during rolling can be regulated from 0° to 26° by changing the angle α between the long axis of the robot and the NIR spot from 0° to 52° (Figure S8e, Supporting Information).

2.9. Versatile Multifunctions

Rapid movement is needed for escaping away from predators and negotiating with uneven terrains. For most crawling terrestrial animals moving on a rough ground, particularly for soft-bodied animals without legs, because it is required to generate and release sufficient energy while minimize the frictional forces.[54] The ATMSRs not only exhibit skillfully employ a rapid action like "pole vaulting" to reach the top of obstacles, when it is blocked by obstacles with a height much larger than that of the ATMSR (**Figure 5**a; and Part 1 of Movie S14, Supporting Information). They also demonstrate fast directional somersaults (Figure S9a,b; and Part 2 of Movie S14, Supporting Information)—a direct mimicry of an escape repertoire used by caterpillars.[55] Moreover, it can also utilize a leaping action to leap over two hurdles which are two and four times higher than its own height (Figure 5b; and Movie S15, Supporting Information), respectively. Moreover, it is remarkable that the ATMSR demonstrates two kinds of powerful high jumping actions: latched high-jumping and buckling-induced high-jumping (details shown in the Supporting Information). Their jumping heights are ≈91 times and 83 times greater than its own height (0.12 mm) (Figure 5c,d; and Part 1 and 2 of Movie S16, Supporting Information), respectively, whereas the jumping height of Mediterranean fruit-fly larvae is ≈39 times higher than the larvae's body height.[56] As shown in Figure 5e, by high jumping, the ATMSR can overcome the obstacles ≈39 times higher than its own height (Part 3 of Movie S16, Supporting Information), which is comparable to that a person of 1.75 m height jumping up to a 24-story building. All these fast motion modes can greatly strengthen the adaptability of the ATMSRs to negotiation challenging environments.

3. Conclusion

In summary, as a kind of novel untethered, miniature mobile soft robot, ATMSRs can swiftly move on all-terrains. They possess the following prominent characteristics: adaptive mobility for diverse challenging terrains, negotiation with various obstacles, exceptional robustness, and versatile multifunction. Our study realizes the engineering of a multidisciplinary system that links soft materials, mechanics, deformation, spatiotemporal, and directional optical stimulation to dynamic locomotive robots. Unlike existing light-driven robots that predetermine the locomotion mode designed at the fabrication stage, the ATMSRs can combine diverse modes of locomotion (lateral rolling, turning, somersaulting, leaping, and high jumping). More importantly they can also flexibly switch among these locomotive modes and thus they can negotiate various types of obstacles and adapt to varying terrains and environments. Owing to the ultrarobustness capabilities, ATMSRs can quickly self-repair and restore mobility even when impacted, punctured or severely distorted in the execution of the task. Additionally, the mobility of the ATMSRs is not compromised or declined when they are covered or stained by dust, sand, soil, and mud. All these unique characteristics indicate exceptional mobility, unprecedented reliability and vigorous vitality of ATMSRs, which are critically important for miniature mobile robots to survive, to retain functions, to execute tasks in harsh environments.

4. Experimental Section

Experimental Materials and Chemicals: NIR-monomer was synthesized by the methods described in the Supporting Information. LC monomer, RM82, was obtained from Bayi Space LCD Technology Co., Ltd. Chain extender (2,2′-(Ethylenedioxy)diethanethiol) and crosslinker (pentaerythritol tetra(3-Mercaptopropionate)) were purchased from TCI Inc. Catalyst (dipropylamine) was obtained from Adamas Reagent Co., Ltd.

Preparation of ATMSRs: Typically, the mixture of NIR-monomer (31.38 mg, 33.03 mmol), LC monomer (200 mg, 297.28 mmol), chain extender (43.01 mg, 235.93 mmol), and crosslinker (23.06 mg, 47.19 mmol) were dissolved in 3 mL dichloromethane (DCM). Thiol groups and acrylate groups were equimolar. One drop of dipropylamine (DPA) was added into the solution of the mixture. Then the mixture was transferred into custom-made Teflon mold (3 × 3 × 0.5 cm^3) quickly. After 5 h curing at room temperature, the partially crosslinked NIR-LCE film was formed and demolded, then stretched to 50% strain to induce LC orientation, keeping the stretching for 24 h to fix the orientation. The oriented NIR- LCE film was cut along short axis of the film to form many small rectangular LCEs (5 × 0.5 × 0.12 mm^3) whose long axis is perpendicular to the nematic director *n*. These rectangular small LCEs were used and developed as ATMSRs.

Characterization: UV–vis–NIR absorption spectra of NIR monomer in dichloromethane solution was recorded using a Shimadzu UV-2700 spectrophotometer. Infrared thermal imager instrument (FLIR-A600-Series, Sweden) was used to observe NIR-induced thermal distribution and intensity. Photomechanical forces were measured using the tensile machine of Instron 5943. For all NIR-light-driven experiments, an NIR

laser source with a wavelength of 808 nm and tunable power output was employed. Laser intenstiy was measured by a power meter (CNI, HS1+TP100). The photographs and videos of the NIR-light-driven experiments were recorded by a super-resolution digital microscope (Keyence, VHX-6000) and digital camera (Canon EOS 80D). The videos of rolling process were recorded by a high-speed microscope VW-9000 at 250.0 fps and analyzed by the software-tracker, a video analysis and modeling tool that enables to trace rolling trajectory.

Supporting Information

Supporting Information is available from the Wiley Online Library or from the author.

Acknowledgements

Conflict of Interest

The authors declare no conflict of interest.

Data Availability Statement

The data that support the findings of this study are available from the corresponding author upon reasonable request.

Keywords

[1] M. Sitti, H. Ceylan, W. Hu, J. Giltinan, M. Turan, S. Yim, E. Diller, *Proc. IEEE* **2015**, *103*, 205.

[2] L. Hines, K. Petersen, G. Z. Lum, M. Sitti, *Adv. Mater.* **2017**, *29*, 1603483.

[3] C. Huang, T. Xu, J. Liu, L. Manamanchaiyaporn, X. Wu, *IEEE Robot. Autom. Lett.* **2019**, *4*, 4185.

[4] W. Hu, G. Z. Lum, M. Mastrangeli, M. Sitti, *Nature* **2018**, *554*, 81.

[5] A. DeMario, J. Zhao, *J. Mech. Robot.* **2018**, *10*, 041005.

[6] C. H. Rhee, J. S. Pulskamp, R. G. Polcawich, K. R. Oldham, *J. Microelectromech. Syst.* **2012**, *21*, 1492.

[7] Y. Wu, J. K. Yim, J. Liang, Z. Shao, M. Qi, J. Zhong, Z. Luo, X. Yan, M. Zhang, X. Wang, R. S. Fearing, R. J. Full, L. Lin, *Sci. Robot.* **2019**, *4*, eaax1594.

[8] K. Okazaki, T. Ogiwara, D. Yang, K. Sakata, K. Saito, Y. Sekine, F. Uchikoba, *Artif. Life Robot.* **2011**, *16*, 229.

[9] B. R. Donald, C. G. Levey, C. D. McGray, I. Paprotny, D. Rus, *J. Microelectromech. Syst.* **2006**, *15*, https://doi.org/10.1109/JMEMS.2005.863697.

[10] J. S. Pulskamp, R. G. Polcawich, R. Q. Rudy, S. S. Bedair, R. M. Proie, T. Ivanov, G. L. Smith, *MRS Bull.* **2012**, *37*, 1062.

[11] S. Nocentini, C. Parmeggiani, D. Martella, D. S. Wiersma, *Adv. Opt. Mater.* **2018**, *6*, 1800207.

[12] R. Murthy, A. N. Das, D. O. Popa, H. E. Stephanou, *Adv. Robot.* **2011**, *25*, 965.

[13] C. Majidi, *Soft Robot.* **2014**, *1*, 5.

[14] S. I. Rich, R. J. Wood, C. Majidi, *Nat. Electron.* **2018**, *1*, 102.

[15] B. Zhang, C. Hu, P. Yang, Z. Liao, H. Liao, *IEEE Robot. Autom. Lett.* **2019**, *4*, 2645.

[16] H. Zeng, P. Wasylczyk, D. S. Wiersma, A. Priimagi, *Adv. Mater.* **2018**, *30*, 1703554.

[17] W. Jiang, D. Niu, H. Liu, C. Wang, T. Zhao, L. Yin, Y. Shi, B. Chen, Y. Ding, B. Lu, *Adv. Funct. Mater.* **2014**, *24*, 7598.

[18] S. Palagi, A. G. Mark, S. Y. Reigh, K. Melde, T. Qiu, H. Zeng, C. Parmeggiani, D. Martella, A. Sanchez-Castillo, N. Kapernaum, F. Giesselmann, D. S. Wiersma, E. Lauga, P. Fischer, *Nat. Mater.* **2016**, *15*, 647.

[19] H. Zeng, P. Wasylczyk, C. Parmeggiani, D. Martella, M. Burresi, D. S. Wiersma, *Adv. Mater.* **2015**, *27*, 3883.

[20] M. Rogoz, H. Zeng, C. Xuan, D. S. Wiersma, P. Wasylczyk, *Adv. Opt. Mater.* **2016**, *4*, 1689.

[21] C. Ahn, X. Liang, S. Cai, *Adv. Mater. Technol.* **2019**, *4*, 1900185.

[22] D. Rus, M. T. Tolley, *Nature* **2015**, *521*, 467.

[23] M. Wehner, R. L. Truby, D. J. Fitzgerald, B. Mosadegh, G. M. Whitesides, J. A. Lewis, R. J. Wood, *Nature* **2016**, *536*, 451.

[24] E. S. Heckscher, S. R. Lockery, C. Q. Doe, *J. Neurosci.* **2012**, *32*, 12460.

[25] R. Y. Hwang, L. Zhong, Y. Xu, T. Johnson, F. Zhang, K. Deisseroth, W. D. Tracey, *Curr. Biol.* **2007**, *17*, 2105.

[26] A. Burgos, K. Honjo, T. Ohyama, C. S. Qian, G. J. Shin, D. M. Gohl, M. Silies, W. D. Tracey, M. Zlatic, A. Cardona, W. B. Grueber, *Elife* **2018**, *7*, e26016.

[27] M. Q. Clark, A. A. Zarin, A. Carreira-Rosario, C. Q. Doe, *Neural Dev.* **2018**, *13*, 6.

[28] C. Aygül, J. Kwiczak-Yiğitbaşi, B. Baytekin, O. Özcan, in *2019 2nd IEEE Intl Conf. on Soft Robotics (RoboSoft)*, IEEE, Seoul, South Korea **2019**, p. 477.

[29] J. Sun, J. Zhao, *IEEE Robot. Autom. Lett.* **2019**, *4*, 724.

[30] J. Zhang, E. Diller, *Soft Robot.* **2018**, *5*, 761.

[31] K. Sugita, D. Tanaka, S. Ono, S. Chiba, K. Iwata, Y. Han, M. Takato, in *2016 IEEE Intl Conf. on Advanced Intelligent Mechatronics (AIM)*, IEEE, Banff, Canada **2016**, p. 431.

[32] T. Ube, T. Ikeda, *Adv. Opt. Mater.* **2019**, *7*, 1900380.

[33] T. J. White, D. J. Broer, *Nat. Mater.* **2015**, *14*, 1087.

[34] J. C. Spagna, D. I. Goldman, P. C. Lin, D. E. Koditschek, R. J. Full, *Bioinspir. Biomim.* **2007**, *2*, 9.

[35] C. Li, A. O. Pullin, D. W. Haldane, H. K. Lam, R. S. Fearing, R. J. Full, *Bioinspir. Biomim.* **2015**, *10*, 046003.

[36] F. Qian, T. Zhang, W. Korff, P. B Umbanhowar, R. J. Full, D. I. Goldman, *Bioinspir. Biomim.* **2015**, *10*, 056014.

[37] M. Anwar, Y. M. Ekhsan, N. Nadzri, L. H. Omar, N. A. Karim, M. Q. Harun, M. A. Jamain, in *2016 2nd Intl. Symp. on Agent, Multi-Agent Systems and Robotics (ISAMSR)*, IEEE, Bangi, Malaysia **2016**, p. 149.

[38] M. Sitti, *Nat. Rev. Mater.* **2018**, *3*, 74.

[39] H. Lu, M. Zhang, Y. Yang, Q. Huang, T. Fukuda, Z. Wang, Y. Shen, *Nat. Commun.* **2018**, *9*, https://doi.org/10.1038/s41467-018-06491-9.

[40] C. Li, P. B. Umbanhowar, H. Komsuoglu, D. E. Koditschek, D. I. Goldman, *Proc. Natl. Acad. Sci. USA* **2009**, *106*, 3029.

[41] C. Li, C. C. Kessens, R. S. Fearing, R. J. Full, *Adv. Robot.* **2017**, *31*, 881.

[42] R. R. Kohlmeyer, J. Chen, *Angew. Chem., Int. Ed.* **2013**, *52*, 9234.

[43] Y. C. Cheng, H. C. Lu, X. Lee, H. Zeng, A. Priimagi, *Adv. Mater.* **2020**, *32*, 1906233.

[44] J. J. Wie, M. R. Shankar, T. J. White, *Nat. Commun.* **2016**, *7*, 13260.

[45] X. Wang, B. Yang, D. Tan, Q. Li, B. Song, Z.-S. Wu, A. del Campo, M. Kappl, Z. Wang, S. N. Gorb, S. Liu, L. Xue, *Mater. Today* **2020**, *35*, 42.

[46] R. Blickhan, R. J. Full, *J. Comp. Physiol. A* **1993**, *173*, 509.

[47] R. Altendorfer, N. Moore, H. Komsuoglu, M. Buehler, H. B. Brown Jr., D. McMordie, U. Saranli, R. Full, D. E. Koditschek, *Auton. Robots* **2001**, *11*, 207.

[48] D. L. Thomsen, P. Keller, J. Naciri, R. Pink, H. Jeon, D. Shenoy, B. R. Ratna, *Macromolecules* **2001**, *34*, 5868.

[49] L. Liu, M. H. Liu, L. L. Deng, B. P. Lin, H. Yang, *J. Am. Chem. Soc.* **2017**, *139*, 11333.

[50] G. Z. Yang, J. Bellingham, P. E. Dupont, P. Fischer, L. Floridi, R. Full, N. Jacobstein, V. Kumar, M. McNutt, R. Merrifield, B. J. Nelson, B. Scassellati, M. Taddeo, R. Taylor, M. Veloso, Z. L. Wang, R. Wood, *Sci. Robot.* **2018**, *3*, eaar7650.

[51] S. Lahiri, K. Shen, M. Klein, A. Tang, E. Kane, M. Gershow, P. Garrity, A. D. T. Samuel, *PLoS One* **2011**, *6*, e23180.

[52] M. Klein, S. V. Krivov, A. J. Ferrer, L. Luo, A. D. T. Samuel, M. Karplus, *Elife* **2017**, *6*, e30503.

[53] H. Zeng, O. M. Wani, P. Wasylczyk, A. Priimagi, *Macromol. Rapid Commun.* **2018**, *39*, 1700224.

[54] A. Harvey, S. Zukoff, *PLoS One* **2011**, *6*, e17746.

[55] H.-T. Lin, G. G. Leisk, B. Trimmer, *Bioinsp. Biomim.* **2011**, *6*, 026007.

[56] D. P. Maitland, *Nature* **1992**, *355*, 159.